Journal of Power Sources 253 (2014) 35–40

Contents lists available at ScienceDirect

Journal of Power Sources

journal homepage: www.elsevier.com/locate/jpowsour

Effects of cathode materials on the characteristics of electrolyte supported micro-tubular solid oxide fuel cells

Wen-Shuo Hsieh [a], Pang Lin [a], Sea-Fue Wang [b,*]

[a] Department of Materials Science and Engineering, National Chiao Tung University, Hsinchu 300, Taiwan, ROC
[b] Department of Materials and Mineral Resources Engineering, National Taipei University of Technology, 1, Sec. 3, Chung-Hsiao E. Rd., Taipei 106, Taiwan, ROC

HIGHLIGHTS

- Properties of tubular SOFC were improved by LSCF–GDC cathode and GDC interlayer.
- The fabrication was improved by carefully monitoring formulation and sintering.
- An LSCF cathode had a power density 44% greater than an LSM cathode.
- Drop in ASR value of LSCF cathode was >30% compared to that of LSM cathode.

ARTICLE INFO

Article history:
Received 27 September 2013
Received in revised form
24 November 2013
Accepted 29 November 2013
Available online 10 December 2013

Keywords:
Solid oxide fuel cell
Tubular
Extrusion
Dip-coating
Interlayer

ABSTRACT

The effects of the GDC–LSCF ($Ce_{0.8}Gd_{0.2}O_{0-\delta}$–$La_{0.6}Sr_{0.4}Co_{0.2}Fe_{0.8}O_{3-\delta}$) cathode layer and the GDC interlayer on the electrochemical performance of the ScSZ ($Zr_{0.8}Sc_{0.2}O_{2-\delta}$) electrolyte supported (≈270 μm) micro-tubular SOFC cells are investigated in this study. Material formulation and sintering profile for fabricating the micro-tubular SOFC cells are developed to avoid physical defects caused by the large sintering shrinkage mismatch among the layers. Cell B (with the LSCF–GDC composite cathode layer and the GDC interlayer) reports an ohmic resistance slightly higher than that of Cell A (with the GDC –$La_{0.8}Sr_{0.2}MnO_{3-\delta}$, i.e. LSM, composite cathode), while its polarization resistance emerges to be significantly smaller than that of Cell A. In terms of cell performance, Cell B demonstrates an OCV value (>1.07 V) similar to that of Cell A and a maximum power density (0.26 W cm^{-2}) 44.4% greater than that of Cell A (0.17 W cm^{-2}) at 850 °C. It can thus be concluded that using the LSCF–GDC composite-cathode layer and inserting the GDC interlayer help reduce the total cell impedance, thereby improving the power density of the tubular cells.

1. Introduction

Solid oxide fuel cell (SOFC) has attracted worldwide interest with its promising commercialization potential thanks to major advantages like high energy conversion efficiency, structural integrity, fuel flexibility, and non-reliance on noble metals of its electrodes [1,2]. To date, planar and tubular designs remain the two most common SOFC configurations. Compared to their planar counterparts, tubular SOFCs are known for superb thermal resistance, secure sealing, solid mechanical strength, rapid heat cycling, and stable performance. The drawbacks, on the other hand, are smaller current density and complex fabrication process [1,3–5]. Considerable efforts have accordingly been invested to reduce cell size and fabricate anode-supported SOFCs with thin electrolytes for raising volumetric power density [6–10]. However, anode-supported tubular SOFCs have often encountered mechanical failure during operation mainly due to the large volume change (around 40 vol.%) of the anode during the reduction and re-oxidation cycles, which may easily crack the thin electrolyte layer and delaminate between the electrode and electrolyte to decrease the cell open circuit voltage (OCV) [11–16].

Using extrusion and dip-coating to prepare electrolyte-supported micro-tubular SOFCs (T-SOFCs), a previous study found the NiO/NiO–ScSZ/ScSZ/GDC–LSM cell exhibiting fine flexural strength (190 MPa), and the micro-tubular SOFCs, after thermal recycling, showed no delamination and retained good mechanical integrity [17]. Yet, the maximum power density (MPD) of the micro-tubular SOFCs reached only 0.23 W cm^{-2} at 900 °C due to the cells' high ohmic and polarization resistances. The ohmic resistance can be reduced by using $Ce_{0.8}Gd_{0.2}O_{0-\delta}$ (GDC) and $La_{0.9}Sr_{0.1}Ga_{0.8}Mg_{0.2}O_{3-\delta}$ (LSGM) as the

* Corresponding author. Tel.: +886 2 2771 2171x2735; fax: +886 2 2731 7185.
E-mail addresses: sfwang@ntut.edu.tw, seafuewang@yahoo.com (S.-F. Wang).

0378-7753/$ – see front matter © 2013 Elsevier B.V. All rights reserved.
http://dx.doi.org/10.1016/j.jpowsour.2013.11.113

electrolyte, which further helps lower the operating temperature [18]. However, the cell performance may be degraded by the impaired mechanical strength or the electronic conduction in the electrolyte. It was shown that the Ce^{4+} ions could be reduced to Ce^{3+} ions under a reducing atmosphere, thereby causing some electronic conduction in the electrolyte and resulting in OCV drop [19]. The high polarization resistance could be reduced by using a single-phase mixed ionic and electronic conductor (MIEC), such as $La_{0.6}Sr_{0.4}Co_{0.2}Fe_{0.8}O_{3-\delta}$ (LSCF), to extend the triple-phase boundary (TPB) into the whole cathode. Unfortunately, LSCF may react with the ZrO_2-based electrolyte over 900 °C, leading to the formation of the performance-degrading $SrZrO_3$ and $La_2Zr_2O_7$ compounds [20–23].

In this study, electrolyte-supported micro T-SOFCs using ScSZ electrolyte and LSCF cathode were fabricated by extrusion and dip-coating. To improve the chemical compatibility between ScSZ and LSCF, a GDC interlayer was inserted between the electrolyte and cathode layers of the NiO/NiO–ScSZ/ScSZ/GDC–LSCF cells [23,24]. The extruded green ScSZ tubes were pre-sintered at 1100 °C and the anode dip-coated onto the inner surfaces of the electrolyte tubes and then sintered at 1400 °C. A NiO current collector layer and a GDC interlayer were then coated respectively onto the inner and outer surfaces of the microtubes before co-sintering at 1350 °C. The fired microtubes consisting of an anode layer, an electrolyte layer, and an interlayer were subsequently dip-coated with the GDC/LSCF cathode and fired at 1200 °C. The NiO/NiO–ScSZ/ScSZ/GDC/GDC–LSCF micro T-SOFCs were built and characterized through microstructural and electrochemical performance studies. The study further investigated and compared the electrochemical performance of the ScSZ-supported micro T-SOFCs using LSCF as the cathode with the electrochemical performance of those with an LSM cathode.

2. Experimental

Fig. 1 presents the schematic drawing of the electrolyte-supported micro T-SOFCs with $La_{0.8}Sr_{0.2}MnO_{3-\delta}$ (LSM) and $La_{0.6}Sr_{0.4}Co_{0.2}Fe_{0.8}O_{3-\delta}$ (LSCF) cathodes. The two designs of micro T-SOFCs used the same half-cell micro-tubes incorporating a $Zr_{0.8}Sc_{0.2}O_{2-\delta}$ (ScSZ) electrolyte tube and a two-layer anode comprising an anode functional layer (AFL) of NiO–ScSZ composite (60 vol.%:40 vol.%) and a current collector layer (outer layer) of pure NiO. For the two designs, Cell A used a $Ce_{0.8}Gd_{0.2}O_{2-\delta}$ (GDC)–LSM composite and Cell B a GDC–LSCF composite as the cathode layer. A GDC interlayer was inserted between the ScSZ electrolyte tube and the GDC–LSCF cathode layer in Cell B to prevent the formation of $SrZrO_3$ and $La_2Zr_2O_7$.

Commercially available raw $Zr_{0.8}Sc_{0.2}O_{2-\delta}$ (ScSZ; d_{50} = 0.09 μm; Fuel Cell Materials) was mixed with binder (Methyl cellulose, MC, Tsair Yu Technology), lubricant (Oil, Tsair Yu Technology, Taiwan), surfactant, and D.I. water. The mixtures were extruded into the micro-tubes with an in-house designed die (diameter = 5 mm). After cutting and drying, the green ScSZ tubes were pre-sintered at 1100 °C. The inner surfaces of the electrolyte tubes were then dip-coated with a NiO (Fuel Cell Materials, d_{50} = 0.8 μm)-ScSZ slurry and then co-fired at 1400 °C. For the preparation of Cell A, the current collector layer of NiO was dip-coated onto the surfaces of the anode functional layer of NiO–ScSZ and subsequently sintered at 1350 °C. The GDC–LSM (20 vol.%:80 vol.%) cathode layer were then dip-coated onto the outer surfaces of the half-cells of the electrolyte-anode micro-tubes in a suspension composed of GDC (Fuel Cell Materials; d_{50} = 0.09 μm) and LSM (Fuel Cell Materials; d_{50} = 1.19 μm) powders, and then post-fired at 1100 °C for 2 h. For the preparation of Cell B, the GDC interlayer was first dip-coated on the outer surfaces of the electrolyte micro-tubes with a green NiO layer in a GDC suspension and then co-sintered at 1350 °C. Finally, the GDC–LSCF (20 vol.%:80 vol.%) cathode were dip-coated onto the surfaces of the GDC interlayer in a GDC–LSCF (Fuel Cell Materials; d_{50} = 0.99 μm) suspension and then post-fired at 1200 °C. Details of the cell preparation are presented elsewhere [18]. In order to evaluate the sintering shrinkage mismatch with respect to temperature for the GDC interlayer and the NiO coated on ScSZ electrolyte tube, dilatometric analysis on the green NiO, green GDC and pre-sintered ScSZ compacts was performed, using a dilatometer (NETZSCH DIL 402C) in air and at a heating rate of 5 °C min^{-1}. The fired ScSZ compact was pre-sintered at 1400 °C for 2 h.

Scanning electron microscopy (SEM, Joel JSM-6510LV) associated with energy dispersive spectroscopy (EDS, INCA X-ACT) was used to conduct chemical analysis and examine the microstructures of the fracture surfaces. The electrochemical performances of the micro T-SOFCs were evaluated using an in-house designed setup. Ag wire and Ni foam were respectively used as cathode and current collector. The micro T-SOFCs were mounted to an alumina tube with hydrogen flowing inside using a sealant (Aremco products, Zirconia 885). The anode was first reduced in H_2 at 700 °C for 1 h. The cell voltage and the power density as a function of cell current density were determined using a potentiostatic instrument (Jiehan ECW-5000) at 800–900 °C at intervals of 50 °C. The impedance analysis was measured by an electrochemical impedance analyzer

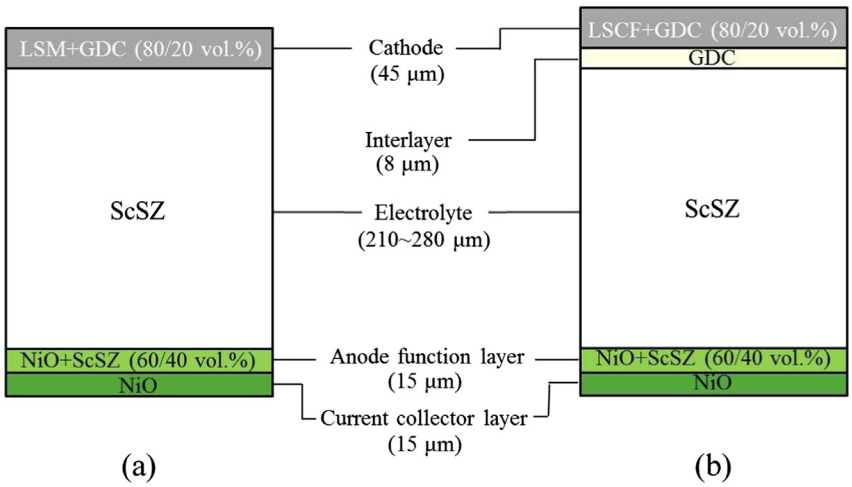

Fig. 1. Schematic drawing of the electrolyte-supported cell structure of micro T-SOFCs: (a) LSM–GDC/ScSZ/NiO–ScSZ/NiO (Cell A); (b) LSCF–GDC/GDC/ScSZ/NiO–ScSZ/NiO (Cell B).

(Jiehan IMS-3522Z) in the frequency range of 0.1–10^4 Hz. The electrochemical impedance analysis and the measurement of cell performances were performed on three samples each for Cell A and Cell B. It was found that the measurements were very reproducible and the deviations of the results appeared to be less than 5%.

3. Results and discussion

Fig. 1 outlines the cell structure of the micro T-SOFCs prepared by this study. To prevent the occurrence of physical defects such as delamination, cracks, pores, and voids in the electrolyte-supported micro T-SOFC cells, the formulation of the electrolyte pastes and the anode and cathode slurries, the tube extrusion and the slurry coating processes, and the firing profiles were carefully monitored [17]. The ScSZ tubes were pre-sintered at 1100 °C before subsequent coating of the anode and cathode onto the inner and outer surfaces of the electrolyte tubes. The firing shrinkage of the electrolyte microtubes was measured to be approximately 26%. The dimension of the fired microtubes used for mechanical support read 20 mm in length and 3.2 mm and 3.7 mm in inner and outer diameters respectively. The maximum flexural strength of the fired microtubes reached approximately 190 MPa, indicating a mechanical strength robust enough in a common operating environment. Cell A, adopting the same design as the one presented in a previous study [18], was composed of a bilayer anode of NiO/NiO–ScSZ, an electrolyte layer of ScSZ, and a composite cathode layer of GDC–LSCF. Different from Cell A, Cell B used a cathode layer of GDC–LSCF and incorporated an additional interlayer of GDC inserted between the electrolyte layer and the cathode layer to inhibit the chemical reaction between LSCF and ScSZ [25]. Fig. 2 displays the appearances of the micro T-SOFCs prepared in this study. The anode was fully covered on the inner surface of the electrolyte microtube, while the cathode was coated over the center portion of the outside surface of the microtube with a length of 5 mm, representing an effective cell area of 0.58 cm^2.

As indicated by Fig. 3 that shows the dilatometric results of the green GDC, green NiO, and pre-sintered ScSZ compacts at a heating rate of 5 °C min^{-1}, at low temperatures, all three samples experienced a slight increase in dimension caused by thermal expansion

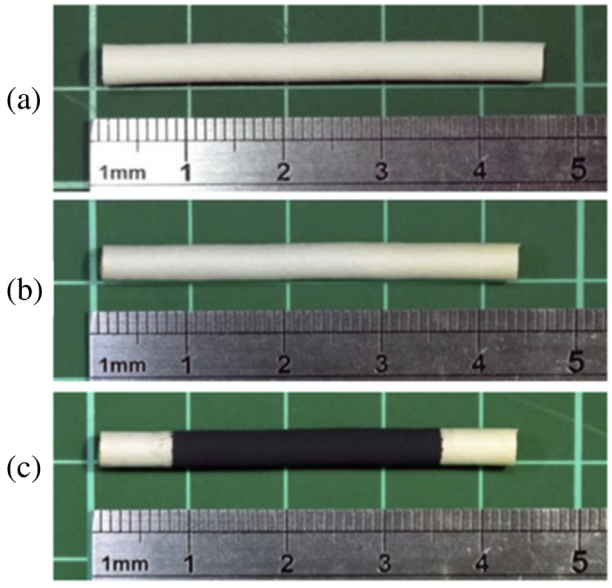

Fig. 2. Images of the micro-tubular SOFC: (a) ScSZ tube pre-sintered at 1100 °C; (b) ScSZ/NiO–ScSZ half-cell substrate; (c) LSCF–GDC/GDC/ScSZ/NiO–ScSZ/NiO micro T-SOFC.

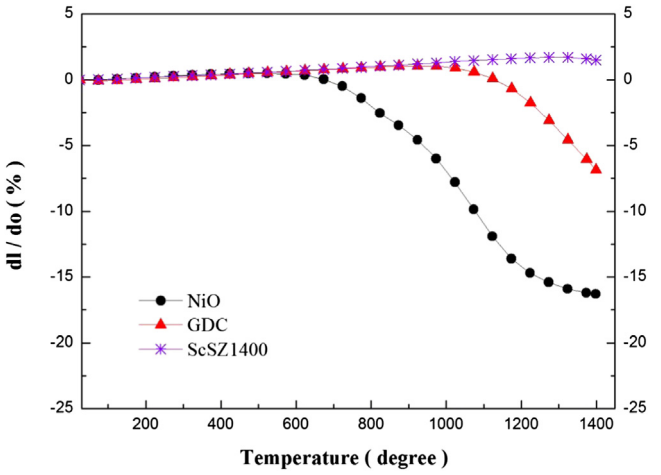

Fig. 3. Dilatometric analysis of the green GDC, green NiO, and pre-sintered ScSZ compacts at a heating rate of 5 °C min^{-1}.

of the ceramics. The GDC compact started to densify at 925 °C, and a total shrinkage of 6.9% was observed as the temperature reached 1400 °C. The NiO compact started to shrink at 525 °C, and the densification finished at approximately 1400 °C with a total shrinkage close to 16.5%. Shrinkage, however, appeared to be negligible for the ScSZ compact pre-sintered at 1400 °C. During the sintering process of the green NiO and GDC layers respectively coated on the inner and outer surfaces of the pre-sintered ScSZ tubes, the pre-sintered ScSZ tubes were expected to show a typical behavior in constraint sintering: exerting a tension force on the GDC and NiO layers when they started to densify. At the sintering temperature of 1400 °C, scaling chip of the NiO layer and axial cracking in the GDC interlayer were detected due to the large shrinkage mismatch. As the sintering temperature declined to 1350 °C, no physical defect on the tubular structure was observed and good mechanical integrity of the microtubes was obtained, which allowed the subsequent coating of the GDC–LSCF cathode layer to be continued.

The SEM microstructures of Cell A can be found in a previous paper [18]. Fig. 4 presents the SEM micrographs of the cross-section of Cell B and the anode microstructure before and after electrochemical measurement. It was observed that the ScSZ electrolyte layer with a thickness of approximately 270 μm was crack free and revealed a dense structure. The interfaces between the electrolyte and electrodes displayed neither discontinuity nor delamination. Compared to its status before the electrochemical measurement [Fig. 4(b)], the anode layer showed a more porous microstructure after the electrochemical measurement [Fig. 4(c)], mainly due to the reduction of NiO to Ni. Similar findings were observed in Cell A. The composition of the anode functional layer, consisting of 60 vol.% NiO and 40 vol.% ScSZ composite, was optimized to display a thermal expansion matching with nearby components and to increase the triple phase boundary (TPB) [26,27]. The thickness of the anode functional layer read 15 μm and showed no notable change after the electrochemical measurement, while the current collector layer (NiO) shrunk from 15 to 10 μm. It indicated that the electrolyte-supported micro T-SOFCs with a thin anode was capable of reducing volume variation due to the reduction–oxidation process during the operation and thus preventing crack formation. This benefit of electrolyte-supported micro T-SOFCs is absent in anode-supported micro T-SOFCs, which are more susceptible to failure caused by crack formation.

Fig. 5 shows the cross-section SEM micrograph and EDS chemical analysis across the cathode-electrolyte interface of Cell B after

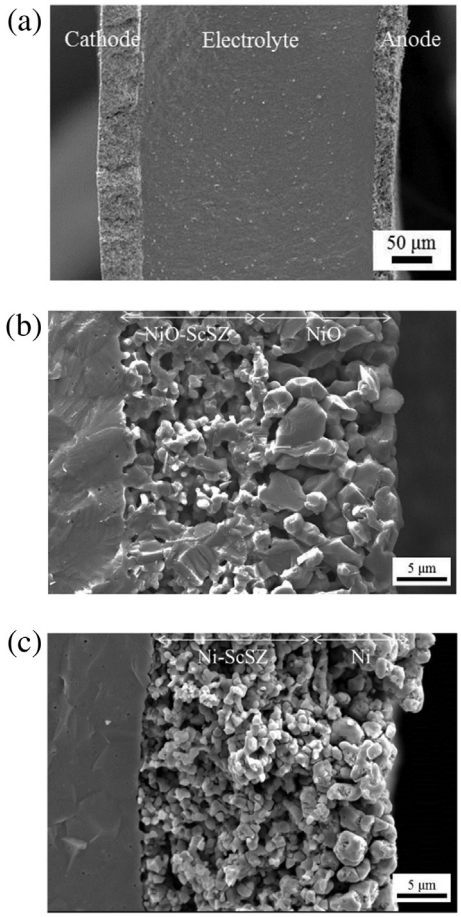

Fig. 4. SEM micrographs of (a) the cross-section of Cell B and the anode microstructure (b) before and (c) after electrochemical measurement.

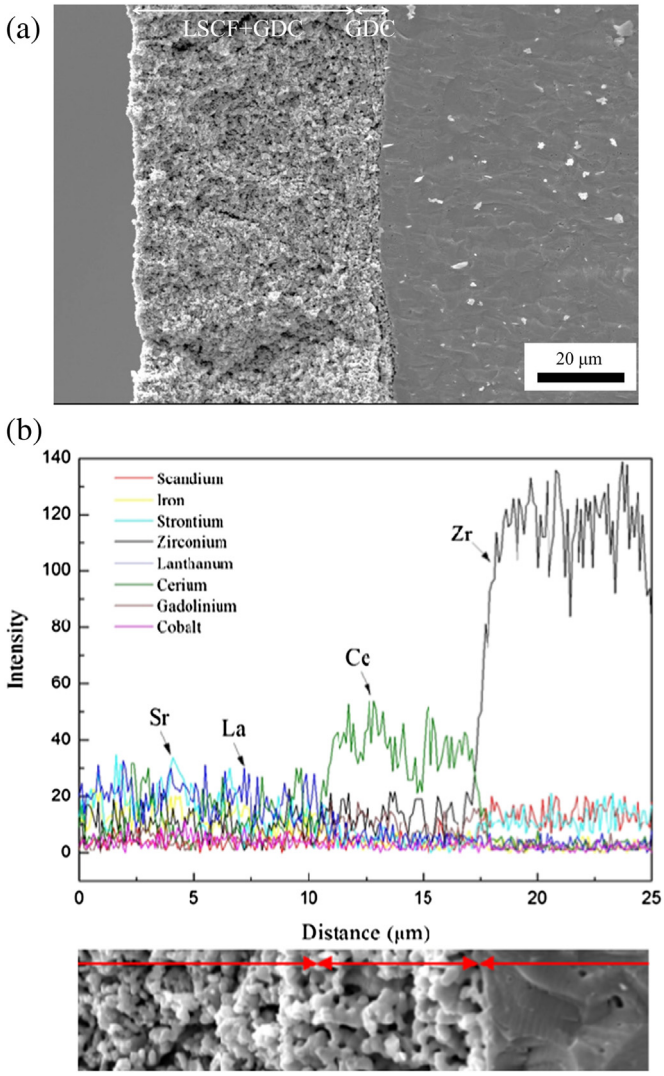

Fig. 5. (a) Cross-section SEM micrograph and (b) EDS chemical analysis across the cathode–electrolyte interface of Cell B after electrochemical measurement at 900 °C.

the electrochemical measurement at 900 °C. The thicknesses of the cathode layer and the interlayer were approximately 40 and 8 μm respectively. The interlayer (GDC) sintered at 1350 °C displayed a porous microstructure and remained firmly attached to the ScSZ electrolyte layer. The porous nature of the GDC interlayer was consistent with similar observations reported in the literature [23–25]. Obtaining a dense GDC interlayer requires a higher sintering temperature of 1500 °C at which severe solid-state reaction occurs between YSZ and GDC [25,28]. According to the EDS result [Fig. 5(b)], no interfacial reaction zone was present; also absent was the inter-diffusion of the Sr and La elements across the interface. Inserting the GDC interlayer thus appeared to successfully impede any chemical interaction between the LSCF cathode and the ScSZ substrate, without inducing any physical defects in cell structure.

Fig. 6 presents the impedance spectra of Cell A and Cell B at 800, 850, and 900 °C, and Table 1 lists the values of ohmic resistance (R_o) obtained from the highest frequency intercept of the impedance spectra and the polarization resistance of the electrode (R_p) determined from the distance between the intercepts of the lowest and the highest frequencies of the impedance spectra. The R_o of the cell includes the resistive contributions of the electrolyte, the two electrodes, the current collectors, and the lead wires. The R_p involves concentration polarization (mass-transfer or gas diffusion polarization) resistance and the effective interfacial polarization resistance associated with the electrochemical reactions at the electrode–electrolyte interface. For Cell A containing an LSM–GDC composite cathode, the ohmic resistances appeared to be 0.66, 0.56, and 0.53 Ω cm^2 and the polarization resistances 3.40, 2.14, and 1.40 Ω cm^2 respectively at 800, 850, and 900 °C. For Cell B containing an LSCF–GDC composite cathode and a GDC interlayer inserted between the electrolyte and the cathode, the ohmic resistances and the polarization resistances emerged to be 0.85, 0.75, and 0.64 Ω cm^2 and 1.55, 1.10, and 0.82 Ω cm^2 respectively at 800, 850, and 900 °C. When compared with Cell A, Cell B revealed at all temperatures apparently higher ohmic resistances but much lower polarization resistances. The additional interface generated by the inserted GDC layer, the porous nature of the GDC interlayer, and the slightly larger thickness of ScSz electrolyte layer (210 and 270 μm respectively for Cell A and Cell B) triggered the higher ohmic resistance of Cell B. On the other hand, using the LSCF–GDC composite cathode lowered the polarization resistance because, compared to the electronic conductor of LSM, LSCF as a mixed ionic and electronic conductor reports a greater electrical conductivity and higher surface oxygen exchange coefficients and oxide-ion diffusivities [22,29]. The mixed ionic–electronic conducting oxide of LSCF also offered more TPB as compared to LSM, even though composite cathodes were adopted in both cases. The decrease in polarization resistance associated with the use of LSCF was significant enough to compensate the increase in ohmic resistance due to the insertion of the GDC interlayer. Overall, the total resistances of Cell B at all temperatures were lower than those of Cell A.

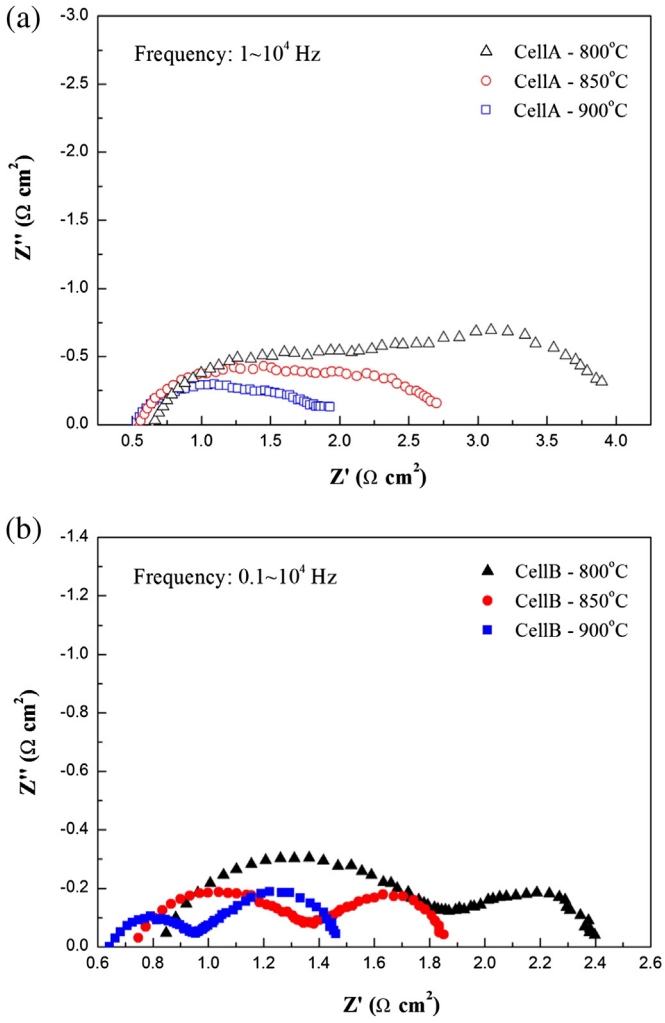

Fig. 6. Impedance spectra of (a) Cell A and (b) Cell B containing interlayer of GDC at 800, 850, and 900 °C.

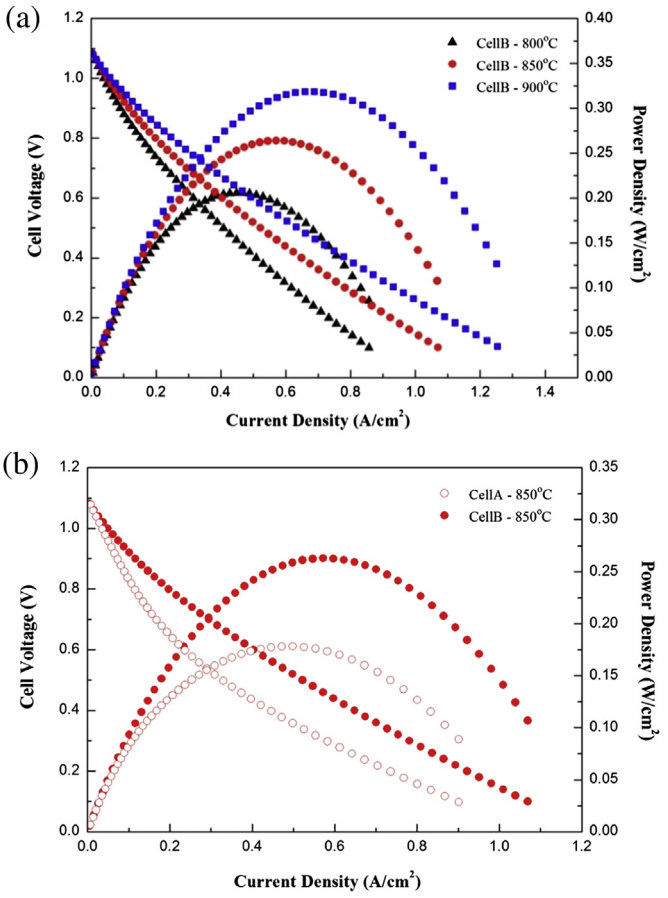

Fig. 7. *I–V* curves and the corresponding power densities of (a) Cell B at different temperatures and (b) Cell B at 850 °C as compared with those of Cell A.

In Fig. 7, the *I–V* curves and the corresponding power densities of Cell B at 800, 850, and 900 °C are presented and compared with those of Cell A at 850 °C. The area specific resistance (ASR) values, as calculated from the initial slope of the *I–V* curve [30], are listed in Table 1. The calculated ASR values at different temperatures were pretty close to the values of total resistance ($R_t = R_o + R_p$). The OCV (open circuit voltage) values of Cell B at different temperatures shown in Fig. 7(a) appeared to be higher than 1.07 V and close to the theoretical value (1.1 V) calculated from the Nernst equation [31], suggesting negligible gas leakage during measurement and testifying to the fine quality of the micro T-SOFCs with a dense and crack-free electrolyte. The maximum power densities (MPDs) of Cell B declined with decreasing operating temperature and emerged to be 0.21, 0.26, and 0.32 W cm^{-2} at 800, 850, and 900 °C respectively. Compared with the performance of Cell A at 850 °C documented in a previous paper [18], Cell B reported similar OCV values but an obviously greater MPD (0.26 W cm^{-2} vs. 0.17 W cm^{-2}) as shown in Fig. 7(b). The 40% increase in the MPD of Cell B was attributed to the significantly lower ASR and, by extension, polarization resistance value. These MPD values are superior to those of the YSZ electrolyte-supported SOFCs reported in the literature [32] and comparable to that (0.26 W cm^{-2}) of a planar type YSZ electrolyte-supported SOFC [33].

Table 1
The ohmic resistance (R_o), polarization resistance (R_p), and area specific resistance (ASR) values of Cell A and Cell B obtained from the impedance spectra shown in Fig. 6.

Sample	Temperature (°C)	R_o (Ω cm^2)	R_p (Ω cm^2)	ASR (Ω cm^2)
Cell A	800	0.66	3.40	4.16
	850	0.56	2.14	2.85
	900	0.53	1.40	2.08
Cell B	800	0.85	1.55	2.41
	850	0.75	1.10	1.86
	900	0.64	0.82	1.47

It can be concluded that inserting the GDC interlayer between the ScSZ electrolyte layer and the LSCF–GDC composite cathode layer is a viable approach for reducing the total cell impedance and thus improve the power density of the tubular cells, if the sintering temperature is low enough to inhibit the chemical interaction between the ScSZ and GDC layers. Further enhancement on the electrochemical performance of the tubular cell might be achieved by thinning the ScSZ electrolyte tube to an extent that it remains robust enough to support the mechanical integrity of the cell. In the planar configuration, though anode-supported SOFCs may benefit from higher power density as a result of the thinned electrolyte layer, electrolyte-supported SOFCs remain the better option in the present SOFC industry for reliability concern since it can minimize the volume change and prevent the formation of defects caused by the reduction/oxidation of Ni during operation. In the tubular configuration, the problems associated with the reduction/oxidation of Ni, notably those related to volume change and stress development, are likely to be more serious and detrimental to the

reliability of the SOFCs. More vigorous R&D efforts are thus needed to further improve the reliability and performance of electrolyte-supported tubular SOFCs in the future.

4. Conclusion

Two types of micro-tubular SOFC cells were fabricated in this study: NiO/NiO–ScSZ/ScSZ/GDC–LSM and NiO/NiO–ScSZ/ScSZ/GDC/GDC–LSCF, designated respectively as Cell A and Cell B. The effects of a GDC interlayer and the associated GDC–LSCF cathode layer on the fabrication techniques and the electrochemical performance of the micro-tubular SOFC cells were investigated. The material formulation and sintering profile of the micro-tubular SOFC cells were carefully monitored to avoid the emergence of physical defects caused by the large sintering shrinkage mismatch among the layers. Compared with Cell A, Cell B reported a slightly higher ohmic resistance (0.75 Ω cm^2 vs. 0.56Ω cm^2) and a significantly smaller polarization resistance (1.10 Ω cm^2 vs. 2.14 Ω cm^2) at 850 °C. Both Cell A and Cell B showed similar OCV values (>1.07 V) but the MPD of the latter (0.26 W cm^{-2}) emerged to be much higher than that of the former (0.17 W cm^{-2}) at 850 °C. Insertion of the GDC interlayer and the use of the LSCF–GDC composite-cathode layer appeared to be capable of effectively improving the cell performance of the tubular SOFC cells.

References

[1] V. Lawlor, S. Griesser, G. Buchinger, A.G. Olabi, S. Cordiner, D. Meissner, J. Power Sources 193 (2009) 387–399.
[2] Yamamoto, Electrochim. Acta 45 (2000) 2423–2435.
[3] S.C. Singhal, Solid State Ionics 135 (2000) 305–313.
[4] J. Van herle, R. Ihringer, N.M. Sammes, G. Tompsett, K. Kendall, K. Yamada, C. Wen, T. Kawada, M. Ihara, J. Mizusaki, Solid State Ionics 132 (2000) 333–342.
[5] K.S. Howe, G.J. Thompson, K. Kendall, J. Power Sources 196 (2011) 1677–1686.
[6] T. Suzuki, Y. Funahashi, T. Yamaguchi, Y. Fujishiro, M. Awano, Electrochem. Solid-State Lett. 10 (2007) 177–179.
[7] S.Y. Park, C.W. Na, J.H. Ahn, U.J. Yun, T.H. Lim, R.H. Song, D.R. Shin, J.H. Lee, J. Power Sources 218 (2012) 119–127.
[8] T. Suzuki, Y. Funahashi, T. Yamaguchi, Y. Fujishiro, M. Awano, J. Power Sources 171 (2007) 92–95.
[9] T. Suzuki, Y. Takahashi, K. Hamamoto, T. Yamaguchi, Y. Fujishiro, Int. J. Hydrogen Energy 36 (2011) 10998–11003.
[10] F. Calise, G. Restuccciaa, N. Sammes, J. Power Sources 195 (2010) 1163–1170.
[11] Faes, A. Hessler-Wyser, A. Zryd, J.V. Herle, Membranes 2 (2012) 585–664.
[12] Faes, A. Nakajo, A. Hessler-Wyser, D. Dubois, A. Brisse, S. Modena, J.V. Herle, J. Power Sources 193 (2009) 55–64.
[13] J.L. Young, V.I. Birss, J. Power Sources 196 (2011) 7126–7135.
[14] H.L. Frandsen, M. Pihlatie, A. Kaiser, D.R. Goldstein, J. Fuel Cell Sci. Technol. 7 (2010) 0510111–0510117.
[15] H. Monzon, M.A. Laguna-Bercero, Int. J. Hydrogen Energy 37 (2012) 7262–7270.
[16] Y.H. Heo, J.W. Lee, S.B. Lee, T.H. Lim, S.J. Park, R.H. Song, C.O. Park, D.R. Shin, Int. J. Hydrogen Energy 36 (2011) 797–804.
[17] W.S. Hsieh, P. Lin, S.F. Wang, Int. J. Hydrogen Energy 38 (2013) 2859–2867.
[18] J.W. Fergus, J. Power Sources 162 (2006) 30–40.
[19] B.C.H. Steele, Solid State Ionics 129 (2000) 95–110.
[20] Sun, R. Hui, J. Roller, J. Solid State Electrochem. 14 (2010) 1125–1144.
[21] L. Qiu, T. Ichikawa, A. Hirano, N. Imanishi, Y. Takeda, Solid State Ionics 158 (2003) 55–65.
[22] J.M. Ralph, C. Rossignol, R. Kumar, J. Electrochem. Soc. 150 (2003) 1518–1522.
[23] Mai, V.A.C. Haanappel, S. Uhlenbruck, F. Tietz, D. Stover, Solid State Ionics 176 (2005) 1341–1350.
[24] Mai, V.A.C. Haanappel, F. Tietz, D. Stover, Solid State Ionics 177 (2006) 2103–2107.
[25] L. Wu, S. Wang, S. Wang, C. Xia, J. Power Sources 240 (2013) 241–244.
[26] D.W. Dees, T.D. Claar, T.E. Easier, D.C. Fee, F.C. Mrazek, J. Electrochem. Soc. 134 (1987) 2141–2146.
[27] T. Matsushima, H. Ohrui, T. Hirai, Solid State Ionics 111 (1998) 315–321.
[28] Martinez-Amesti, A. Larranaga, L.M. Rodriguez-Martinez, M.L. No, J.L. Pizarro, A. Laresgoiti, M.I. Arriortua, J. Power Sources 192 (2009) 151–157.
[29] J.M. Ralph, A.C. Schoeler, M. Krumpelt, J. Mater. Sci. 36 (2001) 1161–1172.
[30] X.D. Zhoua, Electrochem. Soc. Trans. 35 (2011) 1985–1994.
[31] A.J. Bard, L.R. Faulkner, Electrochemical Methods Fundamentals and Applications, Wiley, New York, 2001, p. 31.
[32] C.C. Wei, K. Li, Ind. Eng. Chem. Res. 47 (2005) 1506–1512.
[33] T. Suzuki, M. Awano, P. Jasinski, V. Petrovsky, H.U. Anderson, Solid State Ionics 177 (2006) 2071–2074.